# Lawrence Berkeley National Laboratory

**Title**
Effects of the narrow band gap on the properties of InN

**Permalink**
https://escholarship.org/uc/item/2md4f1mt

**Journal**
Physical Review B, 66(20)

**Authors**
Wu, J.
Walukiewicz, W.
Shan, W.
et al.

**Publication Date**
2002-09-10

Effects of the Narrow Band Gap on the Properties of InN

J. Wu[1,2], W. Walukiewicz[2], W. Shan[2], K.M. Yu[2], J.W. Ager III[2],
E.E. Haller[2,3], Hai Lu[4] and William J. Schaff[4]

1. Applied Science and Technology Graduate Group, University of California, Berkeley, CA 94720.
2. Materials Sciences Division, Lawrence Berkeley National Laboratory, Berkeley, CA 94720.
3. Department of Materials Science and Engineering, University of California, Berkeley, CA 94720.
4. Department of Electrical and Computer Engineering, Cornell University, Ithaca, NY 14853.

Infrared reflection experiments were performed on wurtzite InN films with a range of free electron concentrations grown by molecular beam epitaxy. Measurements of the plasma edge frequencies were used to determine electron effective masses. The results show a pronounced increase in the electron effective mass with increasing electron concentration, indicating a non-parabolic conduction band in InN. We have also found a large Burstein-Moss shift of the fundamental bandgap. The observed effects are quantitatively described by the $k{\cdot}p$ interaction within the two band Kane model of narrow gap semiconductors.

Electronic Mail: w_walukiewicz@lbl.gov

Wurtzite-structured indium nitride forms an alloy with GaN. The alloy on the Ga-rich side is the key component of blue light emitting devices [1]. Early studies of InN films grown by the sputtering method have suggested a direct bandgap of ~ 2 eV [2, 3]. Very recently, optical characterizations of InN crystals grown by molecular beam epitaxy (MBE) [4, 5] or metal-organic vapor phase epitaxy [6] have provided convincing evidence showing that the real bandgap energy of InN is actually about 0.7 eV at room temperature. This value is close to the gap energy of 0.8 eV recently obtained by pseudopotantial calculations [7]. The gap energy of InGaN ternary alloys has been shown to cover a wide, continuous spectral range from the near infrared for InN to the near ultraviolet for GaN [8].

Early measurements of the free electron effective mass in heavily doped ($n > 10^{20}$ cm$^{-3}$) InN films have given a range of values ranging from $0.11m_0$ [2] to $0.24m_0$ [9]. A recent measurement of MBE-grown InN layers ($n = 2.8\times10^{19}$ cm$^{-3}$) using infrared spectroscopic ellipsometry has led to the value of $m^* = 0.14m_0$ [10]. The recently determined low value of the energy gap of InN puts in question and calls for a re-evaluation of the previously determined effective mass. In addition, in the determination of the free carrier effective mass from plasma resonance experiments, the effective mass is inversely proportional to the optical dielectric constant ($e_\infty$) as the plasma frequency is measured [11]. Therefore, it is important to be careful with the choice of $e_\infty$ to compare $m^*$ obtained by different groups.

In this paper we report the results of our studies of the effective mass and the optical absorption edge of wurtzite InN with different free electron concentrations. We find that the lowest conduction band of InN is non-parabolic with the electron effective mass strongly dependent on the electron energy. The optical absorption edge shows a concentration-dependent blue shift resulting from the Burstein-Moss effect. All these observed effects are well described by the two-band Kane model for narrow gap semiconductors.

InN films were grown on (0001) sapphire substrates with an AlN or GaN buffer layer by molecular-beam epitaxy [12]. The thickness of the buffer layer ranges from 70 nm to 200 nm. The InN layer thickness is between 200 nm and 7.5 µm. Although most of the samples were not intentionally doped, free electron concentrations ranging from

$3.5 \times 10^{17}$ cm$^{-3}$ to $5.5 \times 10^{18}$ cm$^{-3}$ have been found in these samples by Hall Effect measurements. Even higher free electron concentrations were achieved by doping InN with Si. The free electron concentration of these doped samples varies between $1.0 \times 10^{19}$ cm$^{-3}$ and $4.5 \times 10^{19}$ cm$^{-3}$. The details of the growth process have been published elsewhere [12]. X-ray diffraction studies have shown that these InN epitaxial layers had high quality and wurtzite structure with their c-axis perpendicular to the substrate surface. Hall mobilities ranged from several hundred up to 2050 cm$^2$/Vs. The samples were characterized by conventional optical absorption and infrared reflection experiments. The optical absorption measurements were performed using a CARY-2390 NIR-VIS-UV spectrophotometer. The infrared reflection experiments were done on a BOMEM DA8 Fourier transform infrared spectrometer with a resolution of 4 cm$^{-1}$. All experiments were carried out at room temperature.

The surface reflection of extrinsic semiconductors in the infrared region by the free carrier plasma is frequently used to determine the effective mass of the free carriers [11]. Similar to the behavior of metals, extrinsic semiconductors strongly reflect infrared light below the plasma frequency. The free carrier effective mass on the Fermi surface can be calculated from the plasma frequency ($w_P$) if the carrier concentration and the optical dielectric constant are known [10, 11].

$$m^* = \frac{ne^2}{e_0 e_\infty w_P^2}. \tag{1}$$

Figure 1 shows, from the left to the right, the infrared reflection curves of three InN samples with free electron concentrations (Hall mobility) of $5.5 \times 10^{18}$ cm$^{-3}$ (615 cm$^2$/Vs), $1.2 \times 10^{19}$ cm$^{-3}$ (1070 cm$^2$/Vs) and $4.5 \times 10^{19}$ cm$^{-3}$ (600 cm$^2$/Vs), respectively. The plasma reflection edge is clearly resolved due to the high electron mobilities in these samples. It can be seen that the plasma reflection edge shifts by as much as 1000 cm$^{-1}$ between these samples. We have used a standard complex dielectric function model that includes finite lifetime broadening to fit the reflection curves [11]. The results are shown as solid curves in Fig. 1. For thick samples with Febry-Perot oscillations, we have also taken into account the optical interference occurring in the epilayer. The plasma frequency and the damping parameter obtained from the fits are 950 cm$^{-1}$ and 100 cm$^{-1}$, 1240 cm$^{-1}$ and 60 cm$^{-1}$, and 1980 cm$^{-1}$ and 250 cm$^{-1}$ for these three samples, respectively.

The electron effective mass calculated from these plasma frequencies are plotted as a function of the electron concentration in Fig. 2. In the calculation, a recently reported isotropically averaged value of the optical dielectric constant, $e_\infty = 6.7$, was used [10]. Also shown in Fig. 2 is the result from Ref.[10] measured with a MBE-grown InN film. The three points with concentration above $10^{20} cm^{-3}$ are effective mass values calculated from the plasma frequencies reported in Ref. [2], [9] and [13] using $e_\infty = 6.7$. In contrast to most semiconductors, the effective mass exhibits a strong dependence on the free electron concentration.

The electron concentration dependent effective mass suggests a non-parabolic conduction band. The conduction band non-parabolicity in other narrow bandgap semiconductors, such as InSb [14] and InAs [15], has been recognized and studied intensively. In these semiconductors the strong conduction band non-parabolicity is attributed to the $k \cdot p$ interaction across the narrow direct gap between the conduction and valence bands. The non-parabolic dispersion relation has been calculated by Kane using a $k \cdot p$ perturbation approach [14]. We have applied Kane's method to InN with a narrow bandgap of 0.7 eV. Since the spin-orbit splitting ($D_{so}$) and crystal field splitting ($D_{cr}$) in the valence bands are extremely small for group III-nitrides [16], we assume them to be practically zero in InN. This approximation is used to estimate the perturbation of the lowest conduction band by the valence bands. Neglecting further perturbations from remote bands, an analytical form of the conduction band dispersion is obtained by solving Kane's two-band $k \cdot p$ model [14],

$$E_C(k) = E_G + \frac{\hbar^2 k^2}{2m_0} + \frac{1}{2}\left( \sqrt{E_G^2 + 4E_P \cdot \frac{\hbar^2 k^2}{2m_0}} - E_G \right) \tag{2}$$

where $E_G$ is the direct bandgap energy, and $E_P$ is an energy parameter related to the momentum matrix element,

$$E_P = \frac{2}{m_0}\left| \langle S|P_x|X \rangle \right|^2. \tag{3}$$

The density of states effective mass is then $k$-dependent and given by [17]

$$m^*(k) = \frac{\hbar^2 k}{dE_C(k)/dk}. \tag{4}$$

The Fermi level is given by the dispersion energy in Eq.(2) evaluated at the Fermi wavevector $k_F = \left(3\boldsymbol{p}^2 n\right)^{1/3}$, neglecting the thermal broadening of the Fermi distribution. We have calculated the effective mass as a function of electron concentration in this model using a bandgap energy $E_G$ = 0.7 eV and $E_P$ equal to 7.5, 10 and 15 eV respectively. The results are compared with experimental data in Fig. 2. It can be seen that although the effective mass data were reported by different groups on InN films grown by different methods, the calculation using $E_P$ = 10 eV shows reasonably good agreement with all the measured data points. For comparison, we note that $E_P$ values for wurtzite GaN as low as 7.7 eV [18] and as high as 14 eV [19] have been reported in the literature. The extrapolation of the curve leads to an effective mass of $0.07m_0$ at the bottom of the conduction band. This value is much smaller than the effective mass of $0.22m_0$ for GaN [11], but is close to $0.08m_0$ for InP [19] that has an almost two times larger band gap.

The non-parabolic dispersion relation of the conduction band also results in an increase of the density of states from that of a parabolic band. It means that the Fermi level rises less rapidly as the lowest conduction band is filled up with electrons. To explore this effect, we have measured the optical absorption edge of InN films with a wide range of free electron concentrations. Typical absorption curves (absorption coefficient squared) are shown in the inset of Fig. 3. It can be seen that although the conduction band is non-parabolic, the absorption can still be approximated by a square-root dependence within ~ 0.05 eV above the onset of the absorption. We extrapolate the linear part of the squared absorption down to the photon energy axis to determine the absorption edge. A strong Burstein-Moss shift of the absorption edge with increasing carrier concentration is observed. The dependence is plotted as solid circles in Fig. 3.

The absorption edge corresponds to the energy of the photons that make vertical transitions from the upper valence band to the Fermi surface in the conduction band. The electron concentration dependence of the absorption edge was calculated based on the non-parabolic dispersion relation given by Eq.(2). In the calculation, the upper valance band involved in the transition is assumed to be parabolic with the hole effective mass equal to the free electron mass in the vacuum [20].

We have also taken into account the conduction band renormalization effects due to the electron-electron interaction and the electron-ionized impurity interaction [21]. The conduction band shift resulting from the electron-electron interaction is given by

$$\Delta E_{e-e} = -\frac{2e^2 k_F}{\boldsymbol{p}\boldsymbol{e}_S} - \frac{e^2 k_{TF}}{2\boldsymbol{e}_S}\left[1 - \frac{4}{\boldsymbol{p}}\arctan\left(\frac{k_F}{k_{TF}}\right)\right], \tag{5}$$

where $k_{TF} = \left(2/\sqrt{\boldsymbol{p}}\right)\left(k_F/a_B\right)^{1/2}$ is the Thomas-Fermi screening wavevector, $\boldsymbol{e}_S$ is the static dielectric constant and $a_B = 0.53\,\boldsymbol{e}_S m_0/m^*$ is the Bohr radius measured in Å. The contribution of the electron-ion interaction to the conduction band shift can written as

$$\Delta E_{e-i} = -\frac{4\boldsymbol{p}e^2 n}{\boldsymbol{e}_S a_B k_{TF}^3}. \tag{6}$$

Both effects are negligible at low electron concentrations. They become quite significant at higher electron concentrations, resulting in a red shift of approximately 0.15 eV per decade of change of $n$ beyond $\sim 10^{19}$ cm$^{-3}$. The calculation shows good agreement with the measured absorption edges, as indicated by the solid curve in Fig. 3. It should be noted that in the calculation no parameter has been adjusted to achieve the good fit. All the values of the parameters (*i.e.*, $E_P$, $E_G$, and $\boldsymbol{e}_\Psi$) used in the calculations of the absorption edge have been determined independently. The results of calculation excluding the band-renormalization effects are also shown as dotted-dashed line in Fig. 3. It can be seen that the increase of the absorption edge energy with electron concentration is too fast as compared to the experimental data if the electron-electron and electron-ionized impurities interactions are ignored. To show the importance of the non-parabolicity of the conduction band on the Moss-Burstein shift, we have also calculated the absorption edge as a function of $n$ assuming a constant electron effective mass of $0.07m_0$ for the conduction band. The results shown as dotted line in Fig. 3 indicate that the conduction band non-parabolicity has to be taken into account to explain the experimentally observed absorption edge shift in InN.

In summary, we have measured the free electron effective mass of InN using plasma reflection in the infrared spectral region. We have found the effective mass to be electron concentration dependent. The dependence can be well described by assuming a non-parabolic conduction band due to the $\boldsymbol{k}\cdot\boldsymbol{p}$ interaction between the conduction band

and valence bands. The Burstein-Moss shift of the absorption edge has also been measured and found to be consistent with the non-parabolic conduction band model.

References

[1] *The Blue Laser Diode*, edited by S. Nakamura and G. Fasol (Springer, Berlin, 1997).

[2]Tyagai, *et. al.*, Sov. Phys. Semicond. **11**, 1257 (1977).

[3]T. L. Tansley and C. P. Foley, J. Appl. Phys. **59**, 3241 (1986).

[4] V. Yu. Davydov, *et. al.*, phys. stat. sol. (b) **229**, R1 (2002).

[5] J. Wu, *et. al.*, Appl. Phys. Lett., **80**, 3967(2002).

[6] Takashi Matsuoka, *et. al.*, Appl. Phys. Lett., **81**, 1246 (2002).

[7] J. L. Li, H .C. Hsueh, and S. G. Louie, to be published.

[8] J. Wu, *et. al.*, Appl. Phys. Lett., **80**, 4741 (2002).

[9] T. Inushima, T. Shiraishi and V. Yu Davydov, Solid State Commun., **110**, 491 (1999).

[10] A. Kasic, *et. al.*, Phys. Rev. B. **65**, 115206 (2002).

[11] P. Perlin, *et. al.*, Appl. Phys. Lett., **68**, 1114 (1996).

[12] H. Lu, *et. al.*, Appl. Phys. Lett., **79**, 1489 (2001).

[13] T. Inushima, *et. al.*, Inst. Phys. Conf. Ser. No. **142**: Chapter 5, p.971.

[14] Evan O. Kane, J. Phys. Chem. Solids, **1**, 249 (1957).

[15] H. A. Washburn, J. R. Sites and H. H. Wieder, J. Appl. Phys., **50**, 4872 (1997).

[16] *e.g.*, $D_{cr}$ and $D_{so}$ for Wurtzite GaN are 10 meV and 18 meV, respectively; see B. Gil, O. Briot and R. Aulombard, Phys. Rev. B **52**, R17028 (1995). Calculated values as small as $D_{cr}$ = 41 meV and $D_{so}$ = 1 meV for InN have been reported in S. H. Wei and A. Zunger, Appl. Phys. Lett., **69**, 2719(1996).

[17] C. Skierbiszewski, *et. al.*, Appl. Phys. Lett., **76**, 2409 (2000).

[18] J. S. Im, *et. al.*, Appl. Phys. Lett., **70**, 631 (1997).

[19] I. Vurgaftman, J. R. Meyer and L. R. Ram-Mohan, J. Appl. Phys., **89**, 5815 (2001).

[20] The calculation results are not sensitive to the value of the hole mass, as it is usually much heavier than the electron effective mass. *e.g.*, a hole effective mass of $1.4m_0$ for GaN has been reported in A. Kasic, *et. al.*, Phys. Rev. B **62**, 7365 (2000).

[21] W. Walukiewicz, *et. al.*, Phys. Rev. B. **41**, 10218 (1990).

Figure Captions

Fig.1 From left to right, infrared reflection curves of three InN samples with free electron concentration of $5.5\times10^{18}$cm$^{-3}$ (thickness 250 nm), $1.2\times10^{19}$cm$^{-3}$ (thickness 7.5 µm) and $4.5\times10^{19}$cm$^{-3}$ (thickness 1.5 µm), respectively. The second and third curves are vertically offset by 0.2 and 0.5, respectively, for clarity. The solid lines are theoretical fits using a standard complex dielectric function model. All experiments were performed at room temperature.

Fig.2. Free electron effective mass as a function of electron concentration. The three points beyond $10^{20}$cm$^{-3}$ are effective mass values calculated from plasma frequencies reported in Ref. [2], [9] and [13] using $\boldsymbol{e}_\infty = 6.7$. The curves are calculated dependences based on Eq.(4) using different $E_P$ values.

Fig.3 Room-temperature absorption edge as a function of free electron concentration. The solid line is the calculated bandgap assuming a non-parabolic ($E_P$=10 eV) dispersion for the conduction band and including the band-renormalization effects. The dotted-dashed line is the same calculation but without including the band-renormalization effects. The dotted line is the result of a calculation assuming a parabolic ($m^*$=0.07 $m_0$) conduction band. Inset: absorption (squared) curves for four samples with different free electron concentrations (in cm$^{-3}$).
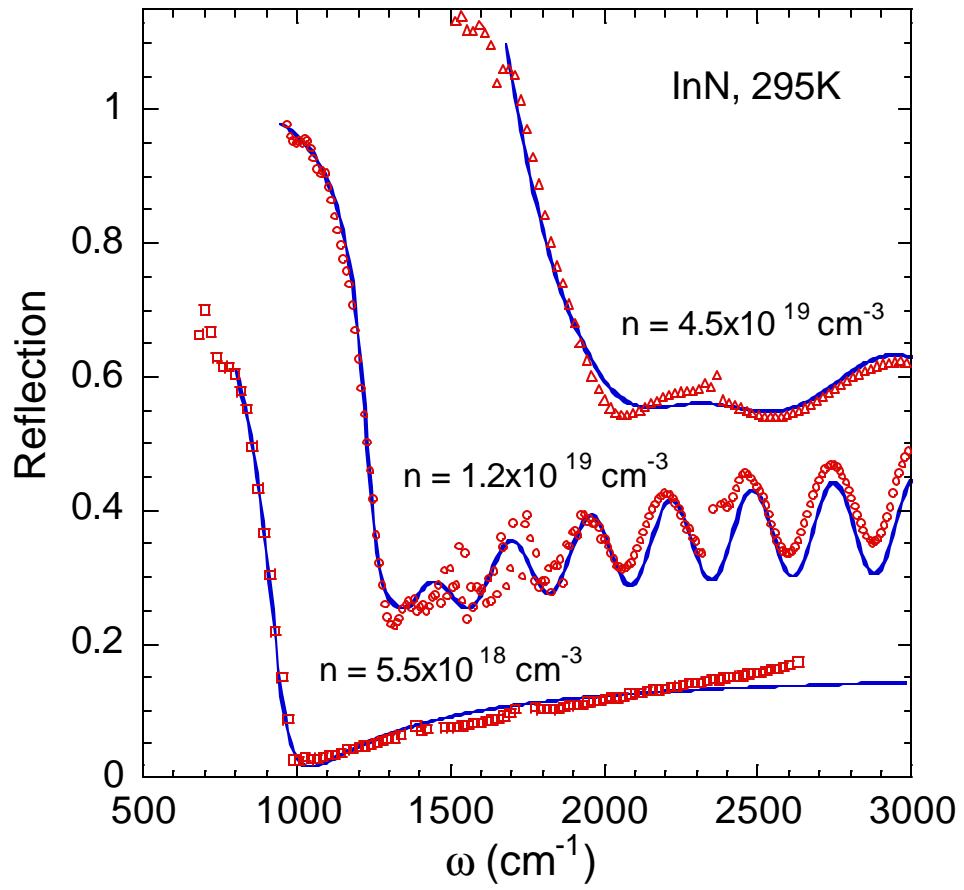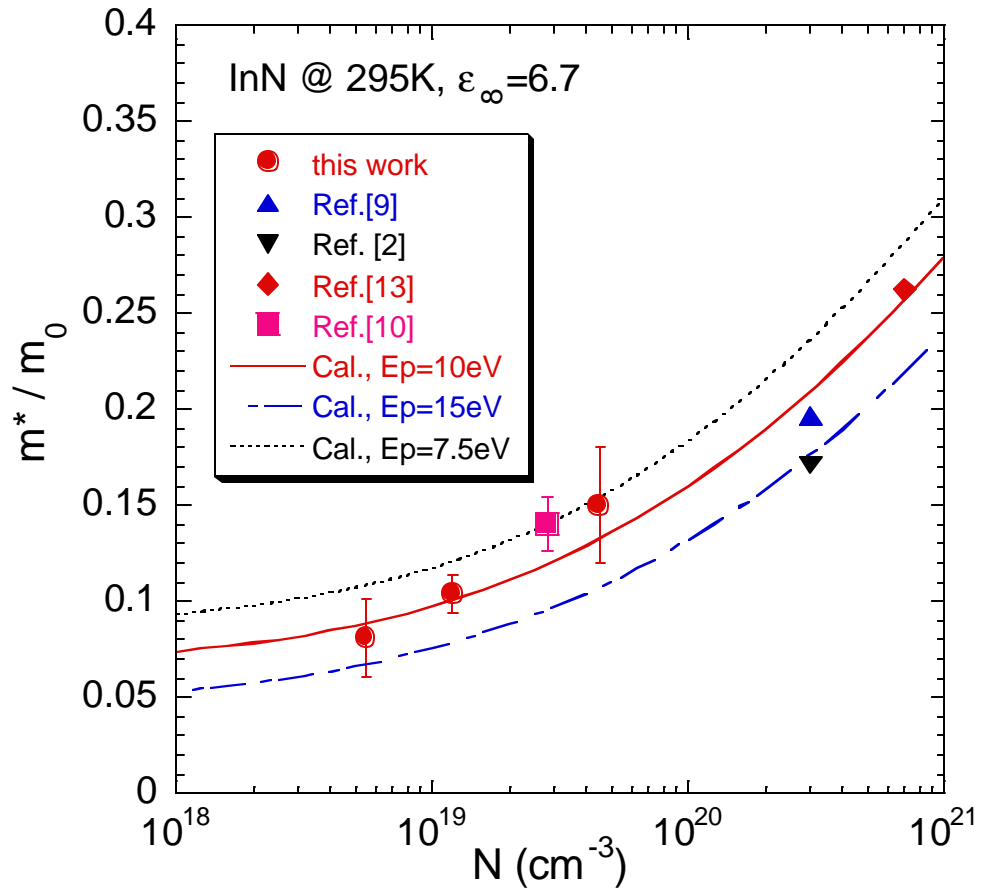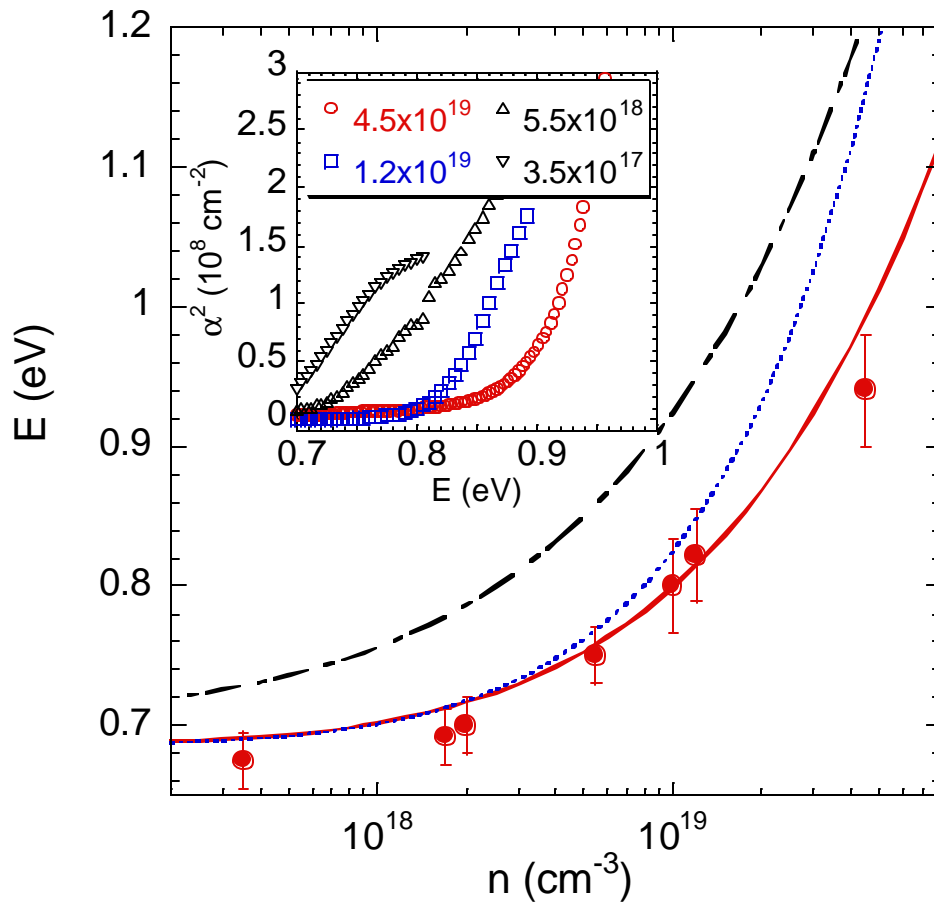
Figures



Fig.1 of 3

J. Wu et. al.

Fig. 2 of 3

J. Wu et. al.

Fig. 3 of 3

J. Wu et. al.